Enhanced photon-pair generation under coherent control

Ke-Shuang Cui, Xiao-Jun Zhang,* and Jin-Hui Wu†
School of Physics and Center for Quantum Sciences, Northeast Normal University, Changchun 130024, China

(Received 8 December 2023; revised 7 April 2024; accepted 6 May 2024; published 3 June 2024)

The generation of the narrowband strong-correlated biphotons via spontaneous four-wave mixing can be effectively controlled and enhanced by an additional driving field which drives a transition with its upper level being a Rydberg state. We study the properties of the noise of the generated biphotons and show that in the region of weak pumping and low atomic density, a high degree of the photon correlation is maintained with the photon-pair generation rate significantly enhanced.

DOI: 10.1103/PhysRevA.109.063701

I. INTRODUCTION

Four-wave mixing is the cornerstone of a wide range of fascinating applications, such as one-atom laser [1], entanglement [2–4], nonlinear optical amplification [5], squeezed light [6], non-Hermitian optical systems [7], and microwave-to-optical conversion [8]. Specifically, the spontaneous four-wave mixing (SFWM) that generates a pair of time-correlated photons in virtue of a third-order nonlinearity [9–12] has driven considerable research efforts. Since the detection of the first photon heralded the arrival of the second one, which was employed in further quantum operation, they have been studied in numerous quantum applications, such as quantum communication [13,14] and quantum memory [15–17].

Improving the pair-generation rate has been a longstanding research focus. It was shown that the efficiency can be effectively increased using the nanostructures [18–20] which confine light resonantly, or by introducing other coherent effects to strengthen the light-matter interaction. For instance, in Ref. [21] the authors proposed a scheme with double pumping fields to construct a quasidark state [21,22] that controlled the ground population to perform the SFWM process near resonance while the Raman process was suppressed. However, such a system supported two sets of SFWM processes that were mixed together and breaks the one-to-one relation between the Stokes and anti-Stokes photons. In another example [23], the interaction between the Rydberg atoms was utilized to enhance the generation efficiency via the nonlocal FWM nonlinearity [24–26]. One potential problem is that the Rydberg interaction needs certain atomic density and the high atomic density usually leads to larger decoherence rates via collisions. This could be fatal to the electromagnetically induced transparency (EIT) [27,28] that suppresses the anti-Stokes photons and reduces the degree of the correlation.

Both of the mentioned works use perturbation theory to model the SFWM process [29], where the evolution operator acts on a vacuum to produce the Stokes–anti-Stokes two-photon state. The absorption of the anti-Stokes photon and the Raman enhancement of the Stokes photon are phenomenologically included as the imaginary parts of the (complex) wave vector. In addition, the fluctuations of the generated photons are neglected. In this paper, we present a theoretical investigation of a modified model with an additional applied driving field forming a "ladder" system together with the pumping field, see Fig. 1(a). We use the field operators to model the generated field, and interaction between the fields and the atoms are depicted by a set of differential equations, rather than the evolution operator in perturbation theory. In this frame which is widely used in the related studies [30–32], the operators of the fluctuations can be easily accounted for and allow us to investigate the noise property of the generated photons. Similar to the model discussed in Ref. [23], a Rydberg state is also included, being the upper level of the transition that the driving field couples. However, we only take advantage of the long-lived time of the level, so that the photons generated by the transitions down from the Rydberg state onto other levels are rare and only one set of SFWM process is supported. As for atomic correlation from the Rydberg-Rydberg interaction, it is negligible due to the weak pumping effect and low Rydberg atomic density that we assume.

The result shows that the presence of the driving field not only provides an effective way to tune the SFWM process, but also significantly increases the generation rate even without atomic correlation. Since the efficiency of the Raman gain and the absorption increase much slower than that of the SFWM nonlinearity, the noises of the generated photons remain at the safe level and the photon correlation is considerably high.

Our paper is organized as follows. In Sec. II we describe our system and derive the dynamical equations for the field operators, with the coefficients of which corresponding to the effects of Raman enhancement, linear absorption, four-wave mixing nonlinearity, and fluctuations. The properties of the coefficients are examined as well. In Sec. III, the influence of the driving field on the generation rate and the correlation between the Stokes and anti-Stokes photons are investigated. We conclude in Sec. IV and the full set of Heisenberg-Langevin equation modeling the properties of the

*zhangxj037@nenu.edu.cn
†jhwu@nenu.edu.cn

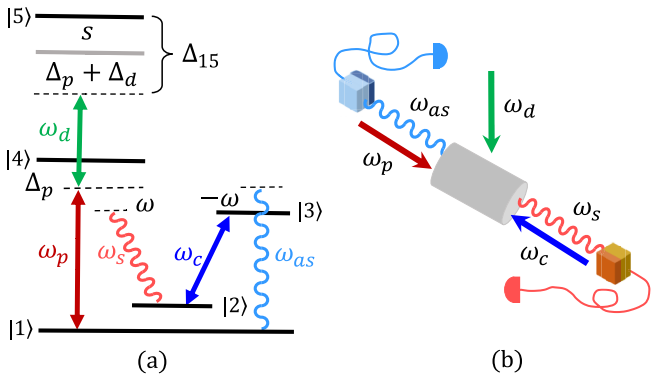

FIG. 1. (a) Energy-level diagram and (b) schematic for spontaneous paired photon generation controlled by a driving field. The sample represented by cylinder is assumed to be a cell of ultra-cold atomic gas ^{87}Rb. The chosen energy levels are $|1\rangle = |5S_{1/2}, F = 1\rangle$, $|2\rangle = |5S_{1/2}, F = 2\rangle$, $|3\rangle = |5P_{1/2}, F = 1\rangle$, $|4\rangle = |5P_{1/2}, F = 2\rangle$, and $|5\rangle$ is a Rydberg level $|60\,S_{1/2}\rangle$.

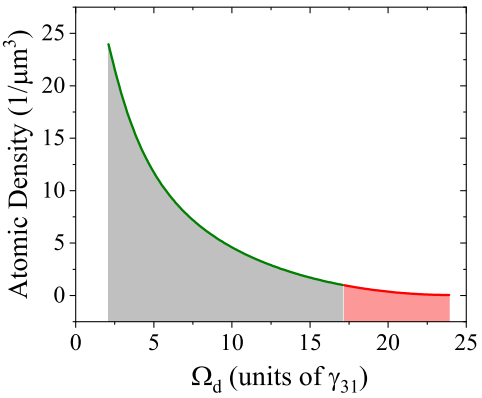

FIG. 2. The maximal atomic density allowed for neglecting the atomic correlation under different driving Rabi frequencies. The gray area and pink area are separated by a white vertical line which indicates the point at $\Omega_d = 17\,\gamma_{31}$ with the corresponding atomic density being $N/V = 1\,\mu\text{m}^{-3}$. Here $\Delta_p = 24\,\gamma_{31}$, $\Delta_c = 0$, $\Delta_{15} = 24\,\gamma_{31}$, $\Omega_p = 1.2\,\gamma_{31}$, $\Omega_c = 3.0\,\gamma_{31}$, $\gamma_{12} = 10^{-3}\,\gamma_{31}$, $\Gamma_{42} = \Gamma_{41} = \Gamma_{32} = \Gamma_{31} = \gamma_{31}$, $\Gamma_{5,4} = \Gamma_{5,3} = 10^{-3}\gamma_{31}$.

atomic gas and the expression of coefficients are presented in Appendixes A, B, and C.

II. MODEL AND EQUATION

Let us consider a group of ultracold five-level atoms, as shown in Fig. 1(a), in the magnetooptical trap where the thermal motion is effectively suppressed so that we do not need to include Doppler broadenings in the following calculation. The pumping field at frequency ω_p drives the transition $|1\rangle \leftrightarrow |4\rangle$, while the coupling field at frequency ω_c, travels in the opposite direction of the pumping [see Fig. 1(b)], and drives $|2\rangle \leftrightarrow |3\rangle$. The corresponding Rabi frequencies of the applied fields are $\Omega_\alpha = \mu_{mn}E_\alpha^+/2\hbar (\alpha \in \{c, p\})$ where μ_{mn} is the dipole moment of the corresponding transition and E_α^+ is the positive-frequency part of the electric field. In virtue of the third-order nonlinearity, a pair of photons is generated spontaneously from the transition $|2\rangle \leftrightarrow |4\rangle$ and $|1\rangle \leftrightarrow |3\rangle$, and we refer to them as the Stokes photon (the one at freqeuncy ω_s) and anti-Stokes photon (at ω_{as}). To suppress the generation of impurity photons from the spontaneous decays and the Raman process, the pumping field is tuned largely off the resonance, i.e., the detuning of the pumping $\Delta_p = \omega_{41} - \omega_p$ is much larger than the decoherence rate γ_{41}. In this way, the Stokes photons are also far away from their resonance and the corresponding absorptions are effectively limited. The coupling field resonates with its transition and creates a window due to electromagnetically induced transparency and allows the anti-Stokes photons to pass through the atomic medium. Traditionally, only the pumping and coupling fields are applied.

In our system, an additional driving field with Rabi frequency Ω_d and frequency ω_d are introduced to couple the transition between $|4\rangle$ and an even higher atomic level $|5\rangle$ which is assumed to be a Rydberg state. The detuning of the driving field is $\Delta_d = \omega_{54} - \omega_d$. We use ω denoting the frequency difference between the pumping field and Stokes photon, $\omega = \omega_p - \omega_s$, then the interaction Hamiltonian reads $\hat{V} = -\hbar\sum_{i=1}^{N}[\Delta_p\hat{\sigma}_{44}^{[i]} + (\Delta_p + \Delta_d)\hat{\sigma}_{55}^{[i]} - \omega\hat{\sigma}_{22}^{[i]} + \omega\hat{\sigma}_{33}^{[i]} + g_{as}\hat{a}_{as}\hat{\sigma}_{31}^{[i]} + g_s\hat{a}_s\hat{\sigma}_{42}^{[i]} + \Omega_c\hat{\sigma}_{32}^{[i]} + \Omega_p\hat{\sigma}_{41}^{[i]} + \Omega_d\hat{\sigma}_{54}^{[i]} + \text{H.c.}] + \frac{1}{2}\sum_{i,j=1}^{N}[\hat{\sigma}_{55}^{[i]}(C_6/|\mathbf{r}_i - \mathbf{r}_j|^6)\hat{\sigma}_{55}^{[j]}]$. N is the number of atoms in the sample. $\hat{\sigma}_{mn}^{[i]} = |m\rangle_{ii}\langle n|$ is the transition operator for the ith atom. Note that the conservation of energy in the four-wave mixing process is already applied in the Hamiltonian. This means the frequency difference between the coupling field and anti-Stokes photon are $\omega_c - \omega_{as} = -\omega$.

For the generated photons, the coupling constant $g_\beta = (\mu_{mn}E_\beta^+)/(2\hbar)$ $(\beta \in \{s, as\})$ and $E_\beta^+ = \sqrt{(\hbar\omega_m)/(2\epsilon_0 V)}$ is the electric field of a single photon. The last term in $\hat{V}$ depicts the interaction between the Rydberg atoms, where $|\mathbf{r}_i - \mathbf{r}_j|$ is the distance between the ith and jth atom, and C_6 is the strength coefficient.

A Rydberg atom prevents the other atoms within a distance of R_b from excited up a Rydberg level. R_b normally referred to as the blockade radius [33] is $R_b = (C_6/\delta_{\text{EIT}})^{1/6}$ with δ_{EIT} being the linewidth of EIT transmission spectrum. In our case with $\Delta_p \gg \gamma_{41}$, $\delta_{\text{EIT}} = |\Omega_d|^2/\Delta_p$. In addition to the Rydberg blockade, the long-range interaction induces correlation $(\langle\hat{\sigma}_{\alpha\beta}^{[i]}\hat{\sigma}_{\mu\nu}^{[j]}\rangle)$ between the states of the two Rydberg atoms, consequently, the nonlocal nonlinearity of the medium [24,25,34]. Such nonlinearity can modify the optical responses of the medium. However, If the Rydberg population is low enough, the modification is negligible. Specifically, if the probability of finding a Rydberg atom in the sphere of $3R_b$ is less than unity, that is,

$$\frac{4}{3}\pi(3R_b)^3\frac{N}{V}\langle\hat{\sigma}_{55}\rangle \leqslant 1, \tag{1}$$

with V being the volume of the atomic cell represented by the cylinder in Fig. 1(b), then we can keep the atomic correlation out of our consideration. Here $\langle\hat{\sigma}_{55}\rangle$ is the population on $|5\rangle$, and it can be obtained from the dynamical equation related to $\hat{V}$ (see the later discussions). Equation (1) can be satisfied if we set a reasonably low atomic density and weak coupling from Ω_p and Ω_d. In Fig. 2 we show the relation between the N/V and Ω_d when the equal sign is taken in the above condition. With the other parameters fixed, the boundary atomic

density is reduced as the driving field becomes stronger. For every point below the curve, the atomic density is safe for neglecting the atomic correlation and our following calculations are valid.

Under such circumstances, the Rydberg atoms are far from each other, and it is reasonable to use mean-field treatment (essentially $\langle\hat{\sigma}_{\alpha\beta}^{[i]}\hat{\sigma}_{\mu\nu}^{[j]}\rangle \simeq \langle\hat{\sigma}_{\alpha\beta}^{[i]}\rangle\langle\hat{\sigma}_{\mu\nu}^{[j]}\rangle$) to replace the Rydberg-Rydberg interaction by an effect shift on the level $|5\rangle$, see Fig. 1(a). The amount of the shift [35,36] is determined by the overall effect of the influence from other nearby excited atoms $s \simeq \frac{N}{V}\int_{R_b}^{\infty}\frac{C_6}{r^6}\langle\hat{\sigma}_{55}\rangle 4\pi r^2 dr$. Thus the effective double-photon detuning of the transition $|1\rangle \leftrightarrow |5\rangle$ is denoted by $\Delta_{15} = s + \Delta_p + \Delta_d$. In this way, we can neglect the Rydberg-Rydberg interaction in the Hamiltonian and the collective slowly varying atomic operators $\hat{\sigma}_{mn} = N^{-1}\sum_{i=1}^{N}|m\rangle_{ii}\langle n|$ evolve according to the Heisenberg-Langevin equation

$$\frac{\partial}{\partial t}\hat{\sigma}_{mn} = \frac{i}{\hbar}[\hat{V}, \hat{\sigma}_{mn}] - \hat{\mathcal{L}}(\hat{\sigma}_{mn}) + \hat{F}_{mn}(z,t), \tag{2}$$

where $\hat{\mathcal{L}}(\hat{\sigma}_{mn})$ is the relaxation matrix including the atomic decay rates of the spontaneous emission and dephasing. $\hat{F}_{mn}$ is the collective atomic δ-correlated Langevin noise operators. Here $\hat{\mathcal{L}}(\hat{\sigma}_{mn})$ and $\hat{F}_{mn}$ are added phenomenally [37]. $\hat{F}_{mn}$ is subject to

$$\langle\hat{F}_{mn}(z,t)\hat{F}_{m'n'}(z',t')\rangle = \frac{L}{N}\mathcal{D}_{mn,m'n'}\delta(t-t')\delta(z-z'), \tag{3}$$

with L being the length of the sample along the propagation of the field. The Langevin diffusion coefficient $\mathcal{D}_{mn,m'n'}$ is determined by the generalized fluctuation-dissipation theorem and Einstein relation, and we list them in Appendix C.

Equation (2) corresponds to a set of differential equations which are presented in Appendix A. Investigating the properties of, e.g., the generation rate of Stoke photons relies on simulating its coupling effect with the anti-Stokes field (nonlinearity of four-wave mixing) and the Raman gain it experienced due to the pumping field. To this end, we need to solve the steady-state equations ($\partial\hat{\sigma}_{ij}/\partial t = 0$) using the standard linearization method [38,39], which in nature is separating the fluctuation from their mean value $\hat{\sigma}_{ij} = \langle\hat{\sigma}_{ij}\rangle + \delta\hat{\sigma}_{ij}$.

Considering that $\langle\hat{a}_s\rangle = \langle\hat{a}_{as}\rangle = 0$, symbols $\delta\hat{a}_s$ and $\delta\hat{a}_{as}$ are not introduced. The mean-value equations only depend on the Rabi frequencies of applied lasers. Also the Rydberg population in the condition (1) and the expression of s, is estimated by the solution $\langle\hat{\sigma}_{55}\rangle$.

For the atomic transitions that generate the Stokes and anti-Stokes photons, the mean valve of σ_{24} and σ_{31} are zeros. Their fluctuations lead to the generation of the biphotons. The polarization corresponding to, e.g., the Stokes field is $\hat{P}_s = 2N\mu_{mn}\delta\hat{\sigma}_{24}$. Then the generation and propagation of the Stokes photons is subject to the Maxwell equation whose Fourier transform reads [40]

$$\frac{\partial\hat{a}_s}{\partial z} + g_R\hat{a}_s + \kappa_s\hat{a}_{as}^{\dagger} = \sum_{\alpha}\xi_{\alpha}^{s}\hat{F}_{\alpha}, \tag{4a}$$

where $g_R(\omega)$ depicts the effect of Raman gain corresponds to the part of $\delta\hat{\sigma}_{24}$ that is proportional to $\hat{a}_s$. In addition, $\kappa_s(\omega)$ is the coefficient of the interaction between the Stokes and anti-Stokes photons; it is derived from the part of $\delta\hat{\sigma}_{24}$ proportional to $\hat{a}_{as}^{\dagger}$. The rest of the $\delta\hat{\sigma}_{24}$ is composed of six

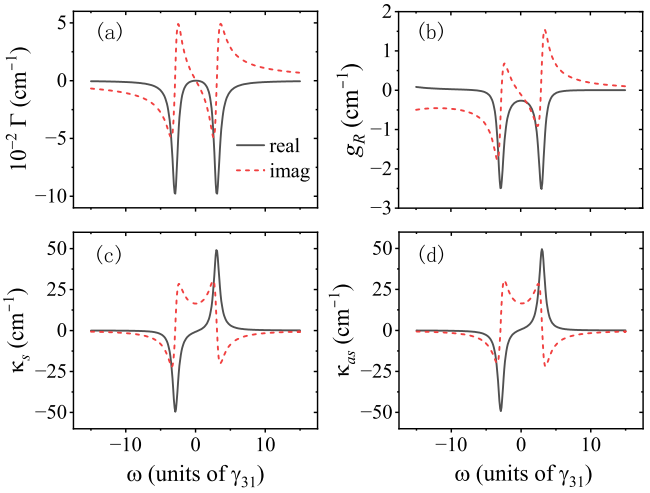

FIG. 3. The (a) coefficient of absorption Γ, (b) Raman enhancement g_R, (c) Stokes and anti-Stokes nonlinear coefficients κ_s, and (d) κ_{as} plotted as the functions of the double photon detuning ω. Here $\Omega_d = 1.2\,\gamma_{31}$, $N = 1.0\times10^{12}$ cm^{-3}, $\sigma = 10^{-9}$ cm^2, and $L = 0.01$ cm. The other parameters are identical with those in Fig. 2.

parts that are respectively proportional to the noise operators $\hat{F}_{21}$, $\hat{F}_{31}$, $\hat{F}_{24}$, $\hat{F}_{34}$, $\hat{F}_{25}$, and $\hat{F}_{35}$. Their contributions to the evolution of the Stokes photons are collected in the right-hand side of Eq. (4) with summation with respect to α is taken over $\alpha \in \{21, 31, 24, 34, 25, 35\}$. A similar equation can be written for the anti-Stokes photons

$$\frac{\partial\hat{a}_{as}^{\dagger}}{\partial z} + \Gamma_{as}\hat{a}_{as}^{\dagger} + \kappa_{as}\hat{a}_s = \sum_{\alpha}\xi_{\alpha}^{as}\hat{F}_{\alpha}. \tag{4b}$$

Here $\Gamma_{as}(\omega)$ is the coefficient linear absorption and $\kappa_{as}(\omega)$ is the coupling coefficient. The coefficients appearing in Eqs. (4a) and (4b) are listed in Appendix B. Note that the coupled equations are not suitable for photon pairs generated by a single Rydberg atom due to the fact that they are derived from Maxwell equation, rather than the Heisenberg equation of motion.

In Fig. 3 we show the value of Γ, g_R, κ_s, and κ_{as} for different ω. As we can see Γ has a typical profile of EIT created by the resonant coupling field. Similar patterns are manifested in the other three coefficients as well. For example, when the absorption of the anti-Stoke photon is large (minimum of Re Γ), the Raman enhancement is severe as well. The valuable region is around the double-photon resonance ($\omega \sim 0$) where the absorption and Raman enhancement is limited and the FWM strength ($|\kappa_s|$, $|\kappa_{as}|$) is still considerable.

The effect of the driving field can be examined by fixing the other parameters and only varying it alone. $|\kappa_s|$ and $|\kappa_{as}|$, as shown in Fig. 4(a), always take the same value for a given value of Ω_d. They increase as Ω_d increases. This implies that the efficiency of the paired-photon generation should be increased as well. However, the absorption and Raman enhancement are enhanced as well. Fortunately, they grow much more slowly.

Such monotonic increments of the four coefficient with respect to Ω_d are better understood if we plot them over a larger range of Ω_d, which are shown in Figs. 4(b) to 4(e). The

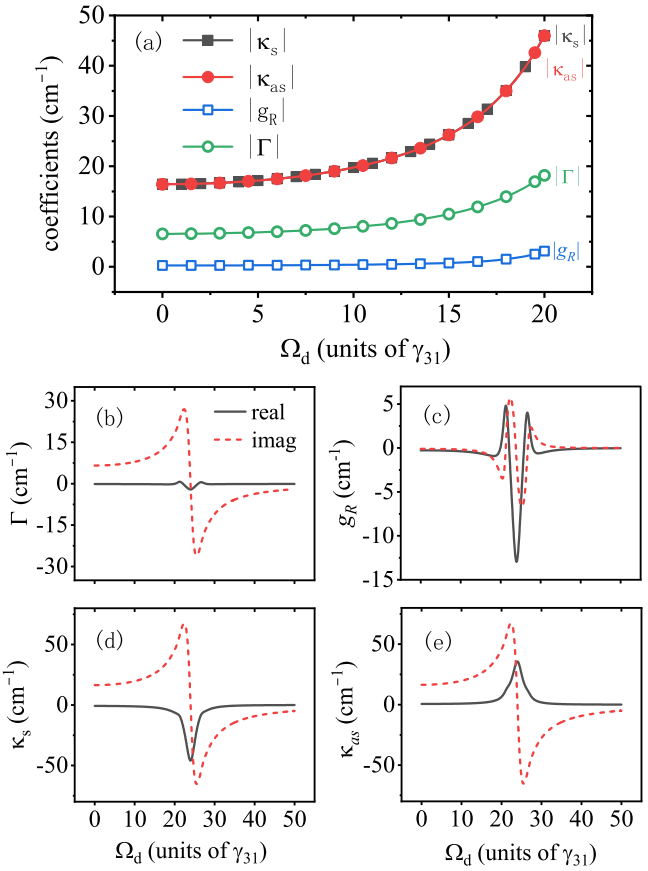

FIG. 4. The relation between the four coefficients and the driving Rabi frequency. (a) $|\Gamma|$, $|g_R|$, $|\kappa_s|$ and $|\kappa_{as}|$ under different driving Rabi frequencies. The real and imaginary parts of the coefficients are shown in (b)–(e) where a wider range of Ω_d is adopted. Here $\omega = 0$, and other parameters are identical with those in Fig. 3.

stronger driven field dynamically shifts the energy level of $|2\rangle$, and makes the coefficients exhibit approximate Lorentz lineshapes as resonances at a particular value of Ω_d, in our case they happen at $\Omega_d = 24\gamma_{31}$. The increment we show in Fig. 4(a) happens on the left-hand side of the resonance. Note that increasing Ω_d causes the population on $|5\rangle$ to increase as well. This might lead to the situation that the influence of the atomic correlation is not negligible anymore due to the enlarged Rydberg interaction. Considering that these four coefficients shown in Figs. 4(b) to 4(e) are proportional to the atomic density, one can always reduce the atomic density to make the atomic correlation reasonably small. This simply scales down the values shown in the figures but the lineshape remains unchanged.

III. GENERATION RATES AND THE CORRELATIONS OF THE BIPHOTONS

The generation rate and the correlation of the biphotons can be obtained from the solution of the Eqs. (4a) and (4b). In the scheme shown in Fig. 1(b) the coupling and pumping fields travel in opposite directions. Thus, according to the phase matching condition ($\mathbf{k}_c + \mathbf{k}_p = \mathbf{k}_s + \mathbf{k}_{as}$) which is assumed to satisfied, the Stokes photon also travels along the opposite direction of the anti-Stokes photon. Thus, $[\hat{a}_s(0), \hat{a}^\dagger_{as}(L)]^T$ should be treated as the boundary condition. The solutions relate to an "evolution" operator

$$\exp[-\mathcal{M}L] = \begin{bmatrix} a & b \\ c & d \end{bmatrix}, \quad \mathcal{M} = \begin{bmatrix} g_R & \kappa_s \\ \kappa_{as} & \Gamma_{as} \end{bmatrix}. \tag{5}$$

The solution of $[\hat{a}_s(L), \hat{a}^\dagger_{as}(0)]^T$ is

$$\begin{bmatrix} \hat{a}_s(L) \\ \hat{a}^\dagger_{as}(0) \end{bmatrix} = \begin{bmatrix} A & B \\ C & D \end{bmatrix} \begin{bmatrix} \hat{a}_s(0) \\ \hat{a}^\dagger_{as}(L) \end{bmatrix} + \sum_\alpha \int_0^L dz \begin{bmatrix} P_\alpha \\ Q_\alpha \end{bmatrix} \hat{F}_\alpha, \tag{6}$$

with

$$\begin{bmatrix} A & B \\ C & D \end{bmatrix} = \begin{bmatrix} a - bc/d & b/d \\ -c/d & 1/d \end{bmatrix}, \tag{7}$$

$$\begin{bmatrix} P_\alpha \\ Q_\alpha \end{bmatrix} = \begin{bmatrix} 1 & -b/d \\ 0 & -1/d \end{bmatrix} e^{\mathcal{M}(z-L)} \begin{bmatrix} \xi^s_\alpha \\ \xi^{as}_\alpha \end{bmatrix}. \tag{8}$$

Then the generation rate of the Stokes photon can be written as

$$R_s = \frac{c}{L} \langle \hat{a}^\dagger_s(L,t) \hat{a}_s(L,t) \rangle, \tag{9}$$

where $\hat{a}_s(L,t)$ is the Fourier transform of the $\hat{a}_s(L)$ [see Eq. (6)]. The frequency dependence of the latter on ω is not explicitly shown. Using the commutation relation $[a_j(z_j,\omega), a^\dagger_j(z_j,\omega')] = L/(2\pi c)\delta(\omega - \omega')$ with $j \in \{s, as\}$ and the correlation $\langle \hat{F}^*_\alpha(\omega, z) \hat{F}_\alpha(\omega', z') \rangle = L/(2\pi N)\mathcal{D}_{\alpha,\alpha^*}\delta(\omega - \omega')\delta(z - z')$, we can rewrite the generation rate as $R_s = \int \frac{d\omega}{2\pi} \tilde{R}_s(\omega)$, with spectral generation rate $\tilde{R}_s$ based on the solution (6) is $\tilde{R}_s(\omega) = |B(\omega)|^2 + \int_0^L \sum_{\alpha,\alpha^*} P^*_\alpha \mathcal{D}_{\alpha^*,\alpha} P_\alpha dz$. Then the generation rate can be written as

$$R_s = R^D_s + R^F_s, \tag{10}$$

with the deterministic part

$$R^D_s = \int \frac{d\omega}{2\pi} |B(\omega)|^2 \tag{11a}$$

and the contribution of the fluctuations is

$$R^F_s = \int \frac{d\omega}{2\pi} \int_0^L \sum_{\alpha,\alpha^*} P^*_\alpha \mathcal{D}_{\alpha^*,\alpha} P_\alpha dz. \tag{11b}$$

The summation with respect to α^* in the above equation originates from $\hat{a}^\dagger_s(L,\omega)$ and $\hat{a}_{as}(0,\omega)$, and it is taken over $\alpha^* \in \{12, 13, 42, 43, 52, 53\}$. For the generation of the anti-Stoke photons, the generation rate is

$$R_{as} = R^D_{as} + R^F_{as}, \tag{12}$$

with

$$R^D_{as} = \int \frac{d\omega}{2\pi} |C(\omega)|^2, \tag{13a}$$

$$R^F_{as} = \int \frac{d\omega}{2\pi} \int_0^L \sum_{\alpha,\alpha^*} Q_\alpha \mathcal{D}_{\alpha,\alpha^*} Q^*_\alpha dz. \tag{13b}$$

Figure 5 shows the generation rates based on Eqs. (11) and (13), plotted as functions of the double-photon detuning ω. If we fix the frequencies of the pumping and coupling field, then ω represents the frequency of the Stokes or anti-Stokes photons. The deterministic part for the Stokes and anti-Stokes

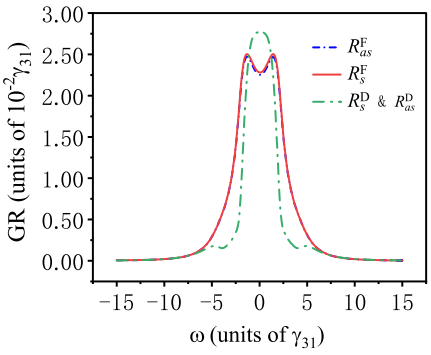

FIG. 5. The relation between the generation rates (GR) and the double-photon detuning. The value of R_s^D and R_{as}^D are approximately equal. The parameters are identical with those in Fig. 3.

take the same value, and the result of fluctuation for the anti-Stokes photon is slightly smaller than that of the Stokes photon at resonance. The linewidth of the biphoton is of the same order as that of optical decoherence rate (e.g., several MHz for Rb atoms), which is quite narrow as compared with that of the spontaneous parametric down-conversion [41].

Since the coefficients of four-wave mixing increase with respect to Ω_d, one would naturally expect that the generation rates should be enhanced when stronger driving field is applied. Such behavior is shown in Fig. 6(a). When $\Omega_d = 0$, which is marked by the black vertical line, the generation rates corresponds to the common scheme without the driving field [29,42]. The existence of the driving field certainly increases the generation rate, see R_s^D and R_{as}^D increasing with Ω_d. In addition, the generation rates without fluctuations, remain identical until the driven field gets too strong. Comparing with the previous studies, such as [21] and [23], the current generation rate is at least three orders of magnitude higher. This is because when exploiting the other effect in the biphoton generation, that is the dark-state effect in Ref. [21] and the Rydberg-Rydberg interation in Ref. [23], the resonant fields are favored. In such a case, the intensity of the applied field should be limited down to certain values to suppress the other unwanted nonlinear process, such as the Raman gain and scattering. Certainly the generation rates are reduced, although increasing the driving field can enhance the biphoton generation. However, the stronger fields also lead to the relatively large Rydberg population and considerable atomic correlation. Suggested by Fig. 2, our theory is valid for Ω_d less than 17 γ_{31}, and the data corresponding to the larger driving Rabi frequency are still informative, but inaccurate.

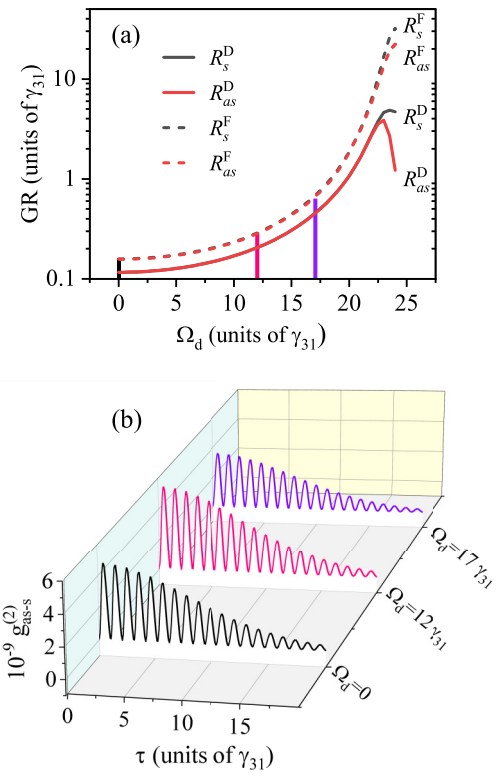

FIG. 6. (a) Generation rates (GR) plotted against the driving Rabi frequency. (b) The normalized cross-correlation function for three particular values of Ω_d which are indicated by the vertical line in (a). The parameters are chosen to be the same as those in Fig. 3.

The correlation between the generated photons can be represented by Glauber's second-order correlation function which is defined as

$$\begin{aligned} G^{(2)}_{as,s}(\tau) &= \langle \hat{a}^{\dagger}_{as}(0,t)\hat{a}^{\dagger}_{s}(L,t+\tau)\hat{a}_{s}(L,t+\tau)\hat{a}_{as}(0,t)\rangle \\ &= R_s R_{as} + |\Phi_{as,s}(\tau)|^2, \end{aligned} \tag{14}$$

with

$$\Phi_{as,s}(\tau) = \frac{L}{c}\mathscr{F}\left(\sum_{\alpha,\alpha^*}\int_0^L dz P_\alpha D_{\alpha,\alpha^*} Q^*_\alpha + AC^*\right). \tag{15}$$

Here $\mathscr{F}$ stands for the Fourier transformation. The quantity that we are interested in is the normalized correlation function $g^{(2)}_{as,s} = 1 + |\Phi_{as,s}(\tau)|^2/(R_s R_{as})$ which is the degree of correlation between Stokes and anti-Stokes photons. The condition for biphoton generation is $g^{(2)}_{as,s} \gg 1$.

We choose three different cases with $\Omega_d = 0$ (transitional four-level system), 12 γ_{31}, and 17 γ_{31} (boundary where the theory applies) to show in Fig. 6(b) the variation of $g^{(2)}_{as,s}$ with respect to the driving field. The larger values of $g^{(2)}_{as,s}$ appear in the case of weaker driving field ($\Omega_d \to 0$). The trade-off between the generation rate and the degree of correlation is clear: overall, $g^{(2)}_{as,s}$ is reduced as Ω_d increases.

Within the scope that our calculations remain reasonable, the degree of the correlation between the Stokes and anti-Stokes photons is considerably high, indicating that the Stokes photon and anti-Stokes photon are strongly correlated. The correlation function oscillates at the frequency of the Ω_c which is a typically effect of EIT-based interaction. The envelope curve of oscillation shows the reduction of the correlation, however the coherence time $t_{\rm coh}$, that is, the time delay at which $g^{(2)}_{as,s}$ decays twice remain approximately the same ($\sim 10\gamma_{31}^{-1}$).

For relatively weak driving, it appears that $R_s^F = R_{as}^F$. This is a result of small decoherence rate between the ground levels ($\gamma_{21} = 10^{-3}\,\gamma_{31}$ in Fig. 6) that we assume. If a hotter atomic gas is used as the sample, then γ_{21} is increased. This leads to imperfect EIT, meaning severe absorption on the anti-Stokes

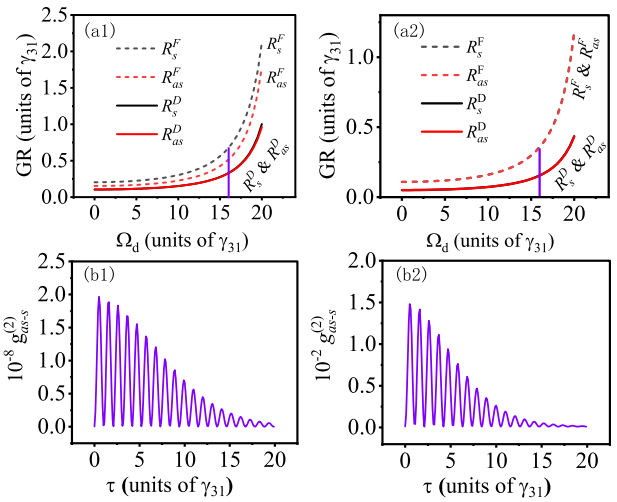

FIG. 7. Generation rates plotted as functions of the driving Rabi frequency with $\gamma_{21} = 0.1\,\gamma_{31}$ and $N/V = 1\,\mu\text{m}^{-3}$ (a1). The vertical line corresponds to $\Omega_d = 17\gamma_{31}$ at which the degree of the photon correlation function is shown in (b1). In (a2) and (b2), $\gamma_{21} = 10^{-3}\,\gamma_{31}$ and $N/V = 0.5\,\mu\text{m}^{-3}$. The parameters are chosen to be the same as those in Fig. 3.

photons. In turn, the generation rate due to fluctuation is enhanced. In Fig. 7(a1) we show the generation rates in the case of $\gamma_{21} = 0.1\gamma_{31}$, As we can see, under the relatively larger decoherence rate, R_s^F deviates from R_{as}^F significantly. This results in an approximately ten times smaller amplitude of the photon correlation in Fig. 7(a2) as compared with the result shown in Fig. 6.

Another noticeable feature in Fig. 6 ($N = 1.0\,\mu\text{m}^{-3}$) is that R_s^F and R_{as}^F are larger than R_s^D and R_{as}^D. The difference between them depends on the atomic density. In Fig. 7(a2) we show the generation rate when a lower atomic density ($N = 0.5\,\mu\text{m}^{-3}$) is chosen. The difference of the generation rate between the noise and the deterministic photon pair gets larger, especially when a larger driving field is applied. One can attribute this property to the relations between the coefficients in Eqs. (4a) and (4b) and the atomic density. κ_s, κ_{as}, g_R, and Γ, see Eqs. (B1) to (B4) in Appendix B are proportional to N, where the coefficient related to the fluctuation $\xi_\alpha^{s/as}$ (listed in Appendix B as well) depends on $\sqrt{N}$. The degree of correlation is dramatically reduced, as shown in Fig. 7(b2). The feature of suppression of noise by increasing atomic density is manifested in the traditionally four-level system as well. In our system with the enhanced generation rate by the coupling field, it is clear that the atomic density should be increased accordingly to suppress the noise. Increasing the length of the atomic sample, leads to the similar result as increasing the atomic density since more atoms participate in generating the biphotons.

IV. CONCLUSION

In this paper, we present a theoretical investigation of the coherent control on the SFWM-based biphoton generation by a driving field. Such a driving field forms a ladder-style three-level subsystem together with the pumping field. To avoid the dark state, the transition between the ground and Rydberg states is largely detuned from its double-photon resonance. By assuming the weak coupling effect of the driving and pumping field, and a relatively law atomic density, we investigate the enhancement and control of the photon pairs in a region where the Rydberg atomic correlation is negligible. Due to the dynamical shift of the intermediate state, the third-order SFWM nonlinear coefficient is enhanced by the driving field and the rate of the increment is larger than that of the Raman gain and absorption. Thus the noise of the generated photons is still under control, although it is increased with the driving field as well. This leads to an enhanced generation rate with relatively high degree of the correlation. For an ever higher intensity of the driving, the effects of the fluctuation become severe, then one need a correspondingly higher atomic density to suppress the noise to maintain the strong photon correlation.

ACKNOWLEDGMENTS

The work is supported by the National Natural Science Foundation of China (Grant No. 12074061).

APPENDIX A: HEISENBERG-LANGEVIN EQUATIONS

Let Γ_m stand for the total decay rate from state $|m\rangle$ and Γ_{mn} is the decay rate from state $|m\rangle$ to state $|n\rangle$. The corresponding dephasing rate γ_{mn} can be written as $\gamma_{54} = \gamma_{45} = (\Gamma_5 + \Gamma_4)/2$, $\gamma_{53} = \gamma_{35} = (\Gamma_5 + \Gamma_3)/2$, $\gamma_{31} = \gamma_{32} = \Gamma_3/2$, $\gamma_{41} = \gamma_{42} = \Gamma_4/2$, and $\gamma_{43} = \gamma_{34} = (\Gamma_4 + \Gamma_3)/2$. Then the atomic transition operators, based on Eq. (2) satisfy the following equations:

$$\partial_t\hat{\sigma}_{11} = \hat{F}_{11} + \Gamma_{41}\hat{\sigma}_{44} + \Gamma_{31}\hat{\sigma}_{33} - i(g_{as}\hat{a}_{as}\hat{\sigma}_{31} + \Omega_p\hat{\sigma}_{41} - g_{as}\hat{a}_{as}^\dagger\hat{\sigma}_{13} - \Omega_p^*\hat{\sigma}_{14});$$

$$\partial_t\hat{\sigma}_{22} = \hat{F}_{22} + \Gamma_{42}\hat{\sigma}_{44} + \Gamma_{32}\hat{\sigma}_{33} - i(\Omega_c\hat{\sigma}_{32} + g_s\hat{a}_s\hat{\sigma}_{42} - \Omega_c^*\hat{\sigma}_{23} - g_s\hat{a}_s^\dagger\hat{\sigma}_{24});$$

$$\partial_t\hat{\sigma}_{33} = \hat{F}_{33} - (\Gamma_{32} + \Gamma_{31})\hat{\sigma}_{33} + \Gamma_{53}\hat{\sigma}_{55} - i(g_{as}\hat{a}_{as}^\dagger\hat{\sigma}_{13} + \Omega_c^*\hat{\sigma}_{23} - g_{as}\hat{a}_{as}\hat{\sigma}_{31} - \Omega_c\hat{\sigma}_{32});$$

$$\partial_t\hat{\sigma}_{44} = \hat{F}_{44} - (\Gamma_{42} + \Gamma_{41})\hat{\sigma}_{44} + \Gamma_{54}\hat{\sigma}_{55} - i(\Omega_p^*\hat{\sigma}_{14} + \Omega_d\hat{\sigma}_{54} + g_s\hat{a}_s^\dagger\hat{\sigma}_{24} - \Omega_p\hat{\sigma}_{41} - \Omega_d^*\hat{\sigma}_{45} - g_s\hat{a}_s\hat{\sigma}_{42});$$

$$\partial_t\hat{\sigma}_{55} = \hat{F}_{55} - (\Gamma_{53} + \Gamma_{54})\hat{\sigma}_{55} - i(\Omega_d^*\hat{\sigma}_{45} - \Omega_d\hat{\sigma}_{54});$$

$$\partial_t\hat{\sigma}_{54} = \hat{F}_{54} - (\gamma_{54} - i\Delta_d)\hat{\sigma}_{54} - i(\Omega_d^*\hat{\sigma}_{44} - \Omega_p\hat{\sigma}_{51} - g_s\hat{a}_s\hat{\sigma}_{52} - \Omega_d^*\hat{\sigma}_{55});$$

$$\partial_t\hat{\sigma}_{51} = \hat{F}_{51} - (\gamma_{51} - i\Delta_{15})\hat{\sigma}_{51} - i(\Omega_d^*\hat{\sigma}_{41} - g_{as}\hat{a}_{as}^\dagger\hat{\sigma}_{53} - \Omega_p^*\hat{\sigma}_{54});$$

$$\partial_t\hat{\sigma}_{41} = \hat{F}_{41} - (\gamma_{41} - i\Delta_p)\hat{\sigma}_{41} - i(\Omega_p^*\hat{\sigma}_{11} + g_s\hat{a}_s^\dagger\hat{\sigma}_{21} + \Omega_d\hat{\sigma}_{51} - g_{as}\hat{a}_{as}^\dagger\hat{\sigma}_{43} - \Omega_p^*\hat{\sigma}_{44});$$

$$\partial_t\hat{\sigma}_{32} = \hat{F}_{32} - (\gamma_{32} - i\Delta_c)\hat{\sigma}_{32} - i(g_{as}\hat{a}_{as}^\dagger\hat{\sigma}_{12} + \Omega_c^*\hat{\sigma}_{22} - \Omega_c^*\hat{\sigma}_{33} - g_s\hat{a}_s^\dagger\hat{\sigma}_{34});$$

$$\partial_t\hat{\sigma}_{25} = \hat{F}_{25} - [\gamma_{25} + i(\Delta_{15} + \omega)]\hat{\sigma}_{25} - i(\Omega_c\hat{\sigma}_{35} + g_s\hat{a}_s\hat{\sigma}_{45} - \Omega_d\hat{\sigma}_{24});$$

$$\partial_t\hat{\sigma}_{35} = \hat{F}_{35} - [\gamma_{35} + i(\Delta_{15} + \omega - \Delta_c)]\hat{\sigma}_{35} - i(g_{as}\hat{a}_{as}^\dagger\hat{\sigma}_{15} + \Omega_c^*\hat{\sigma}_{25} - \Omega_d\hat{\sigma}_{34});$$

$$\partial_t\hat{\sigma}_{24} = \hat{F}_{24} - [\gamma_{24} + i(\Delta_p + \omega)]\hat{\sigma}_{24} - i[\Omega_c\hat{\sigma}_{34} + g_s\hat{a}_s(\hat{\sigma}_{44} - \hat{\sigma}_{22}) - \Omega_p\hat{\sigma}_{21} - \Omega_d^*\hat{\sigma}_{25}];$$

$$\partial_t\hat{\sigma}_{34} = \hat{F}_{34} - [\gamma_{34} + i(\Delta_p + \omega - \Delta_c)\hat{\sigma}_{34}] - i(g_{as}\hat{a}_{as}^\dagger\hat{\sigma}_{14} + \Omega_c^*\hat{\sigma}_{24} - \Omega_p\hat{\sigma}_{31} - \Omega_d^*\hat{\sigma}_{35} - g_s\hat{a}_s\hat{\sigma}_{32});$$

$$\partial_t\hat{\sigma}_{21} = \hat{F}_{21} - (\gamma_{21} + i\omega)\hat{\sigma}_{21} - i(\Omega_c\hat{\sigma}_{31} + g_s\hat{a}_s\hat{\sigma}_{41} - g_{as}\hat{a}_{as}^\dagger\hat{\sigma}_{23} - \Omega_p^*\hat{\sigma}_{24});$$

$$\partial_t\hat{\sigma}_{31} = \hat{F}_{31} - [\gamma_{31} + i(\omega - \Delta_c)\hat{\sigma}_{31}] - i[g_{as}\hat{a}_{as}^\dagger(\hat{\sigma}_{11} - \hat{\sigma}_{33}) + \Omega_c^*\hat{\sigma}_{21} - \Omega_p^*\hat{\sigma}_{34}].$$

APPENDIX B: COEFFICIENTS IN THE STOKES-ANTI-STOKES COUPLED EQUATIONS

The coefficients that appear in Eqs. (4a) and (4b) are quite complex. However, they can be written in relatively compact forms if expressed in terms of the mean values

$$\Gamma = -i\mathcal{N}\sigma\gamma_{31}\Omega^{-1}(\mathscr{A}_1\langle\hat{\sigma}_{22}\rangle + \mathscr{A}_2\langle\hat{\sigma}_{32}\rangle + \mathscr{A}_5\langle\hat{\sigma}_{41}\rangle - \mathscr{A}_1\langle\hat{\sigma}_{44}\rangle + \mathscr{A}_3\langle\hat{\sigma}_{45}\rangle); \tag{B1}$$

$$\kappa_s = -i\mathcal{N}\sigma\gamma_{31}\Omega^{-1}(\mathscr{B}_1\langle\hat{\sigma}_{22}\rangle + \mathscr{B}_3\langle\hat{\sigma}_{32}\rangle + \mathscr{B}_5\langle\hat{\sigma}_{41}\rangle - \mathscr{B}_1\langle\hat{\sigma}_{44}\rangle + \mathscr{B}_4\langle\hat{\sigma}_{45}\rangle); \tag{B2}$$

$$\kappa_{as} = -i\mathcal{N}\sigma\gamma_{31}\Omega^{-1}(\mathscr{A}_6\langle\hat{\sigma}_{11}\rangle - \mathscr{A}_2\langle\hat{\sigma}_{14}\rangle + \mathscr{A}_4\langle\hat{\sigma}_{15}\rangle - \mathscr{A}_5\langle\hat{\sigma}_{23}\rangle - \mathscr{A}_6\langle\hat{\sigma}_{33}\rangle); \tag{B3}$$

$$g_R = -i\mathcal{N}\sigma\gamma_{31}\Omega^{-1}(\mathscr{B}_6\langle\hat{\sigma}_{11}\rangle - \mathscr{B}_3\langle\hat{\sigma}_{14}\rangle + \mathscr{B}_2\langle\hat{\sigma}_{15}\rangle - \mathscr{B}_5\langle\hat{\sigma}_{23}\rangle - \mathscr{B}_6\langle\hat{\sigma}_{33}\rangle), \tag{B4}$$

where $\mathcal{N} = N/V$ is the atomic density and σ is the absorption cross section of the atom. We define complex quantities $g_1 = \gamma_{21} + i\omega$, $g_2 = \gamma_{24} + i(\omega + \Delta_p)$, $g_3 = \gamma_{25} + i(\omega + \Delta_{15})g_4 = \gamma_{31} + i(\omega - \Delta_c)$, $g_5 = \gamma_{34} + i(-\Delta_c + \omega + \Delta_p)$, $g_6 = \gamma_{35} + i(-\Delta_c + \omega + \Delta_{15})$ to collect decoherence rate and detunings together. After introducing a symbol to represent the product of those quantities $g_{\alpha\beta\gamma\ldots} = g_\alpha g_\beta g_\gamma \ldots$, then Ω, $\mathscr{A}_\alpha$, and $\mathscr{B}_\alpha$ in the above equations can be expressed as follows: $\Omega = g_{23}|\Omega_c\Omega_d|^2 - 2|\Omega_c|^4|\Omega_d|^2 + g_{25}|\Omega_c|^4 + g_{2356}|\Omega_c|^2$, $\mathscr{A}_1 = ig_3|\Omega_c\Omega_d|^2 + ig_5|\Omega_c|^4 + ig_{356}|\Omega_c|^2$, $\mathscr{A}_2 = -\Omega_c|\Omega_c\Omega_d|^2 + g_{36}\Omega_c|\Omega_c|^2 + |\Omega_c|^4\Omega_c$, $\mathscr{A}_3 = g_{56}|\Omega_c|^2\Omega_d - |\Omega_c|^4\Omega_d + |\Omega_c\Omega_d|^2\Omega_d$, $\mathscr{A}_4 = -ig_3|\Omega_c|^2\Omega_c\Omega_d - ig_5|\Omega_c|^2\Omega_c\Omega_d$, $\mathscr{A}_5 = |\Omega_c\Omega_d|^2\Omega_p - g_{36}|\Omega_c|^6|\Omega_p|^2 + g_{3456}\Omega_p$, $\mathscr{A}_6 = -ig_3\Omega_c|\Omega_d|^2\Omega_p - ig_5|\Omega_c|^2\Omega_c\Omega_p - ig_{356}\Omega_c\Omega_p$, $\mathscr{B}_1 = ig_3\Omega_c\Omega_d^2\Omega_p + ig_5|\Omega_c|^2\Omega_c\Omega_p + ig_{356}\Omega_c\Omega_p$, $\mathscr{B}_2 = -ig_3|\Omega_c|^2\Omega_d\Omega_p - ig_5|\Omega_c|^2\Omega_d\Omega_p$, $\mathscr{B}_3 = -|\Omega_c\Omega_d|^2\Omega_p + g_{36}|\Omega_c|^2\Omega_p + |\Omega_c|^4\Omega_p$, $\mathscr{B}_4 = g_{56}\Omega_c\Omega_d\Omega_p$, $\mathscr{B}_5 = -g_{23}\Omega_c|\Omega_d|^2 - g_{25}|\Omega_c|^2\Omega_c - g_{2356}\Omega_c$, $\mathscr{B}_6 = -ig_{356}|\Omega_p|^2$,

The coefficient of the noise operators are

$$\xi_{21}^{as} = 2i\sqrt{\mathcal{N}\sigma\gamma_{31}}\Omega^{-1}(-ig_{56}\Omega_c|\Omega_d|^2 - ig_{25}|\Omega_c|^2\Omega_c - ig_{2356}\Omega_c)$$
$$\xi_{24}^{as} = 2i\sqrt{\mathcal{N}\sigma\gamma_{31}}\Omega^{-1}(g_5|\Omega_c|^2\Omega_c\Omega_p + g_{356}\Omega_c\Omega_p),$$
$$\xi_{25}^{as} = 2i\sqrt{\mathcal{N}\sigma\gamma_{31}}\Omega^{-1}(ig_{56}\Omega_c\Omega_d\Omega_p + i\Omega_c|\Omega_d|^2\Omega_d\Omega_p),$$
$$\xi_{21}^{s} = 2i\sqrt{\mathcal{N}\sigma\gamma_{31}}\Omega^{-1}(ig_{3456}\Omega_p - ig_{36}|\Omega_c|^2\Omega_p),$$
$$\xi_{24}^{s} = 2i\sqrt{\mathcal{N}\sigma\gamma_{31}}\Omega^{-1}(g_3|\Omega_c\Omega_d|^2 + g_{356}|\Omega_c|^2),$$
$$\xi_{25}^{s} = 2i\sqrt{\mathcal{N}\sigma\gamma_{31}}\Omega^{-1}(ig_{56}|\Omega_c|^2\Omega_d + i|\Omega_c|^2|\Omega_d|^2\Omega_d),$$
$$\xi_{31}^{as} = 2i\sqrt{\mathcal{N}\sigma\gamma_{31}}\Omega^{-1}(g_5|\Omega_c\Omega_p|^2 + g_{356}|\Omega_p|^2)$$
$$\xi_{34}^{as} = 2i\sqrt{\mathcal{N}\sigma\gamma_{31}}\Omega^{-1}(i|\Omega_c\Omega_d|^2\Omega_p - ig_{36}|\Omega_c|^2\Omega_p)$$
$$\xi_{35}^{as} = 2i\sqrt{\mathcal{N}\sigma\gamma_{31}}\Omega^{-1}(g_3|\Omega_c|^2\Omega_d\Omega_p + g_5|\Omega_c|^2\Omega_d\Omega_p)$$
$$\xi_{31}^{s} = 2i\sqrt{\mathcal{N}\sigma\gamma_{31}}\Omega^{-1}(g_3\Omega_c|\Omega_d|^2\Omega_p + g_{356}\Omega_c\Omega_p)$$
$$\xi_{34}^{s} = 2i\sqrt{\mathcal{N}\sigma\gamma_{31}}\Omega^{-1}(i|\Omega_c|^2\Omega_c\Omega_d^2 - ig_{36}|\Omega_c|^2\Omega_c)$$
$$\xi_{35}^{s} = 2i\sqrt{\mathcal{N}\sigma\gamma_{31}}\Omega^{-1}(g_5|\Omega_c|^2\Omega_c\Omega_d + g_3|\Omega_c|^2\Omega_c\Omega_d).$$

APPENDIX C: DIFFUSION COEFFICIENTS

The collective Langevin noise operators are defined, in the similar way of the collective slowly varying atomic operators, as

$$\hat{F}_{mn}(z,t) = \frac{1}{N}\sum_{i\in N}\hat{F}_{mn}^{[i]}(t), \tag{C1}$$

where $\hat{F}_{mn}^{[i]}(t)$ is the Langevin noise operator for the ith atom. $\hat{F}_{mn}(z,t)$ is subject to the correlation of

$$\langle \hat{F}_{mn}(t,z)\hat{F}_{m'n'}(t',z')\rangle = \frac{L}{N}\mathcal{D}_{mn,m'n'}(t,z)\delta(t-t')\delta(z-z'). \tag{C2}$$

In the frequency domain the noise correlation is

$$\langle \hat{F}_{mn}(\omega,z)\hat{F}_{m'n'}(\omega',z')\rangle = \frac{L}{2\pi N}\mathcal{D}_{mn,m'n'}\delta(\omega-\omega')\delta(z-z'). \tag{C3}$$

The diffusion coefficients $\mathcal{D}_{mn,m'n'}$, based on the generalized fluctuation-dissipation theorem and Einstein relation, can be obtained from the relation

$$\mathcal{D}_{mn,m'n'} = \mathscr{D}(\hat{\sigma}_{mn}\hat{\sigma}_{m'n'}) - \mathscr{D}(\hat{\sigma}_{mn})\hat{\sigma}_{m'n'} - \hat{\sigma}_{mn}\mathscr{D}(\hat{\sigma}_{m'n'}). \tag{C4}$$

The notation $\mathscr{D}(\hat{\sigma}_{mn})$ denotes the deterministic part of the Heisenberg equation of motion for $\hat{\sigma}_{mn}$ (equations in Appendix A without the fluctuation operators). Then those for the noise of the Stokes photons are

$$\begin{aligned}
&\mathcal{D}_{12,24} = \gamma_{12}\langle\hat{\sigma}_{14}\rangle, && \mathcal{D}_{12,25} = \gamma_{12}\langle\hat{\sigma}_{15}\rangle, && \mathcal{D}_{13,31} = \Gamma_{41}\langle\hat{\sigma}_{44}\rangle + \Gamma_{31}\langle\hat{\sigma}_{33}\rangle + (\Gamma_{31}+\Gamma_{32})\langle\hat{\sigma}_{11}\rangle,\\
&\mathcal{D}_{13,34} = (\Gamma_{31}+\Gamma_{32})\langle\hat{\sigma}_{14}\rangle, && \mathcal{D}_{13,35} = \Gamma_{31}+\Gamma_{32}\langle\hat{\sigma}_{15}\rangle, && \mathcal{D}_{42,21} = \gamma_{21}\langle\hat{\sigma}_{41}\rangle,\\
&\mathcal{D}_{42,24} = \Gamma_{54}\langle\hat{\sigma}_{55}\rangle, && \mathcal{D}_{43,31} = (\Gamma_{31}+\Gamma_{32})\langle\hat{\sigma}_{41}\rangle, && \mathcal{D}_{43,34} = \Gamma_{54}\langle\hat{\sigma}_{55}\rangle + (\Gamma_{31}+\Gamma_{32})\langle\hat{\sigma}_{44}\rangle,\\
&\mathcal{D}_{43,35} = (\Gamma_{31}+\Gamma_{32})\langle\hat{\sigma}_{45}\rangle, && \mathcal{D}_{52,21} = \gamma_{21}\langle\hat{\sigma}_{51}\rangle, && \mathcal{D}_{53,31} = (\Gamma_{31}+\Gamma_{32})\langle\hat{\sigma}_{51}\rangle,\\
&\mathcal{D}_{53,34} = (\Gamma_{31}+\Gamma_{32})\langle\hat{\sigma}_{54}\rangle, && \mathcal{D}_{53,35} = (\Gamma_{31}+\Gamma_{32})\langle\hat{\sigma}_{55}\rangle. &&
\end{aligned}$$

Those for the anti-Stokes photons are

$$\begin{aligned}
&\mathcal{D}_{21,12} = \Gamma_{32}\langle\hat{\sigma}_{33}\rangle + \Gamma_{42}\langle\hat{\sigma}_{44}\rangle + 2\gamma_{21}\langle\hat{\sigma}_{22}\rangle, && \mathcal{D}_{21,13} = \gamma_{21}\langle\hat{\sigma}_{23}\rangle,\\
&\mathcal{D}_{31,12} = \gamma_{12}\langle\hat{\sigma}_{32}\rangle, && \mathcal{D}_{31,13} = \Gamma_{53}\langle\hat{\sigma}_{55}\rangle,\\
&\mathcal{D}_{24,42} = \gamma_{32}\langle\hat{\sigma}_{33}\rangle + \gamma_{42}\langle\hat{\sigma}_{44}\rangle + (\Gamma_{41}+\Gamma_{42})\langle\hat{\sigma}_{22}\rangle, && \mathcal{D}_{24,43} = (\Gamma_{41}+\Gamma_{42})\langle\hat{\sigma}_{23}\rangle,\\
&\mathcal{D}_{25,52} = \Gamma_{32}\langle\hat{\sigma}_{33}\rangle + \Gamma_{42}\langle\hat{\sigma}_{44}\rangle + (\Gamma_{53}+\Gamma_{54})\langle\hat{\sigma}_{22}\rangle, && \mathcal{D}_{25,53} = (\Gamma_{53}+\Gamma_{54})\langle\hat{\sigma}_{23}\rangle,\\
&\mathcal{D}_{35,52} = (\Gamma_{53}+\Gamma_{54})\langle\hat{\sigma}_{32}\rangle, && \mathcal{D}_{35,53} = \Gamma_{53}\langle\hat{\sigma}_{55}\rangle + (\Gamma_{53}+\Gamma_{54})\langle\hat{\sigma}_{33}\rangle,\\
&\mathcal{D}_{34,43} = \Gamma_{53}\langle\hat{\sigma}_{55}\rangle + (\Gamma_{41}+\Gamma_{42})\langle\hat{\sigma}_{33}\rangle, && \mathcal{D}_{34,42} = (\Gamma_{41}+\Gamma_{42})\langle\hat{\sigma}_{32}\rangle.
\end{aligned}$$

[1] J. McKeever, A. Boca, A. Boozer, J. Buck, and H. Kimble, Experimental realization of a one-atom laser in the regime of strong coupling, Nature (London) **425**, 268 (2003).

[2] Y. Wu, M. G. Payne, E. W. Hagley, and L. Deng, Preparation of multiparty entangled states using pairwise perfectly efficient single-probe photon four-wave mixing, Phys. Rev. A **69**, 063803 (2004).

[3] F. Wang, C. Wang, K. Shen, and X. Hu, Stable entanglement and one-way steering via engineering of a single-atom reservoir, Opt. Express **30**, 15830 (2022).

[4] V. Boyer, A. M. Marino, R. C. Pooser, and P. D. Lett, Entangled images from four-wave mixing, Science **321**, 544 (2008).

[5] H.-C. Li, G.-Q. Ge, and M. S. Zubairy, Achieving nonlinear optical modulation via four-wave mixing in a four-level atomic system, Phys. Rev. A **97**, 053826 (2018).

[6] C. F. McCormick, V. Boyer, E. Arimondo, and P. D. Lett, Strong relative intensity squeezing by four-wave mixing in rubidium vapor, Opt. Lett. **32**, 178 (2007).

[7] Y. Jiang, Y. Mei, Y. Zuo, Y. Zhai, J. Li, J. Wen, and S. Du, Anti-parity-time symmetric optical four-wave mixing in cold atoms, Phys. Rev. Lett. **123**, 193604 (2019).

[8] J. P. Covey, A. Sipahigil, and M. Saffman, Microwave-to-optical conversion via four-wave mixing in a cold ytterbium ensemble, Phys. Rev. A **100**, 012307 (2019).

[9] H. Takesue and K. Inoue, Generation of polarization-entangled photon pairs and violation of Bell's inequality using spontaneous four-wave mixing in a fiber loop, Phys. Rev. A **70**, 031802(R) (2004).

[10] S. Mittal, V. V. Orre, E. A. Goldschmidt, and M. Hafezi, Tunable quantum interference using a topological source of indistinguishable photon pairs, Nat. Photon. **15**, 542 (2021).

[11] L. Zatti, J. E. Sipe, and M. Liscidini, Generation of photon pairs by spontaneous four-wave mixing in linearly uncoupled resonators, Phys. Rev. A **107**, 013514 (2023).
[12] S. Du, J. Wen, and M. H. Rubin, Narrowband biphoton generation near atomic resonance, J. Opt. Soc. Am. B **25**, C98 (2008).
[13] S. Ritter, C. Noelleke, C. Hahn, A. Reiserer, A. Neuzner, M. Uphoff, M. Muecke, E. Figueroa, J. Bochmann, and G. Rempe, An elementary quantum network of single atoms in optical cavities, Nature (London) **484**, 195 (2012).
[14] K.-F. Chang, T.-P. Wang, C.-Y. Chen, Y.-H. Chen, Y.-S. Wang, Y.-F. Chen, Y.-C. Chen, and I. A. Yu, Low-loss high-fidelity frequency beam splitter with tunable split ratio based on electromagnetically induced transparency, Phys. Rev. Res. **3**, 013096 (2021).
[15] M. P. Hedges, J. J. Longdell, Y. Li, and M. J. Sellars, Efficient quantum memory for light, Nature (London) **465**, 1052 (2010).
[16] Z. Yu, Z. Wu, X. Li, X. Feng, W. Huang, K. Zhang, C.-H. Yuan, W. Zhang, and L. Q. Chen, Interferometry-integrated noise-immune quantum memory, Phys. Rev. Lett. **131**, 150804 (2023).
[17] P.-J. Tsai, Y.-F. Hsiao, and Y.-C. Chen, Quantum storage and manipulation of heralded single photons in atomic memories based on electromagnetically induced transparency, Phys. Rev. Res. **2**, 033155 (2020).
[18] M. Kues, C. Reimer, P. Roztocki, L. R. Cortes, S. Sciara, B. Wetzel, Y. Zhang, A. Cino, S. T. Chu, B. E. Little, D. J. Moss, L. Caspani, J. Azana, and R. Morandotti, On-chip generation of high-dimensional entangled quantum states and their coherent control, Nature (London) **546**, 622 (2017).
[19] H. Takesue, Y. Tokura, H. Fukuda, T. Tsuchizawa, T. Watanabe, K. Yamada, and S.-i. Itabashi, Entanglement generation using silicon wire waveguide, Appl. Phys. Lett. **91**, 201108 (2007).
[20] S. Azzini, D. Grassani, M. Galli, L. C. Andreani, M. Sorel, M. J. Strain, L. G. Helt, J. E. Sipe, M. Liscidini, and D. Bajoni, From classical four-wave mixing to parametric fluorescence in silicon microring resonators, Opt. Lett. **37**, 3807 (2012).
[21] H.-M. Zhao, X.-J. Zhang, M. Artoni, G. C. La Rocca, and J.-H. Wu, Photon-pair generation on resonance via a dark state, Phys. Rev. A **106**, 023711 (2022).
[22] M. O. Scully and M. S. Zubairy, *Quantum Optics* (Cambridge University Press, Cambridge, Englan, 1997).
[23] H.-M. Zhao, X.-J. Zhang, M. Artoni, G. C. La Rocca, and J.-H. Wu, Biphoton generation enhanced by nonlocal nonlinearity via Rydberg interactions, Opt. Lett. **48**, 5105 (2023).
[24] J. D. Pritchard, D. Maxwell, A. Gauguet, K. J. Weatherill, M. P. A. Jones, and C. S. Adams, Cooperative atom-light interaction in a blockaded Rydberg ensemble, Phys. Rev. Lett. **105**, 193603 (2010).
[25] Z. Bai and G. Huang, Enhanced third-order and fifth-order Kerr nonlinearities in a cold atomic system via Rydberg-Rydberg interaction, Opt. Express **24**, 4442 (2016).
[26] Y. Mu, L. Qin, Z. Shi, and G. Huang, Giant Kerr nonlinearities and magneto-optical rotations in a Rydberg-atom gas via double electromagnetically induced transparency, Phys. Rev. A **103**, 043709 (2021).
[27] K.-J. Boller, A. Imamoğlu, and S. E. Harris, Observation of electromagnetically induced transparency, Phys. Rev. Lett. **66**, 2593 (1991).
[28] M. Fleischhauer, A. Imamoglu, and J. P. Marangos, Electromagnetically induced transparency: Optics in coherent media, Rev. Mod. Phys. **77**, 633 (2005).
[29] J. Wen, Y.-H. Zhai, S. Du, and M. Xiao, Engineering biphoton wave packets with an electromagnetically induced grating, Phys. Rev. A **82**, 043814 (2010).
[30] V. Balić, D. A. Braje, P. Kolchin, G. Y. Yin, and S. E. Harris, Generation of paired photons with controllable waveforms, Phys. Rev. Lett. **94**, 183601 (2005).
[31] J. Wen and M. H. Rubin, Transverse effects in paired-photon generation via an electromagnetically induced transparency medium. II. beyond perturbation theory, Phys. Rev. A **74**, 023809 (2006).
[32] A. V. Sharypov and A. D. Wilson-Gordon, Narrowband-biphoton generation due to long-lived coherent population oscillations, Phys. Rev. A **84**, 033845 (2011).
[33] M. Saffman, T. G. Walker, and K. Mølmer, Quantum information with Rydberg atoms, Rev. Mod. Phys. **82**, 2313 (2010).
[34] X.-J. Zhang, H. Chang, J.-Y. Huo, and J.-H. Wu, Enhanced nonlinearity of four-wave mixing via Rydberg-Rydberg interactions, New J. Phys. **24**, 103002 (2022).
[35] D. Ma, D. Yu, X.-D. Zhao, and J. Qian, Unidirectional and controllable higher-order diffraction by a Rydberg electromagnetically induced grating, Phys. Rev. A **99**, 033826 (2019).
[36] B. J. DeSalvo, J. A. Aman, C. Gaul, T. Pohl, S. Yoshida, J. Burgdörfer, K. R. A. Hazzard, F. B. Dunning, and T. C. Killian, Rydberg-blockade effects in Autler-Townes spectra of ultracold strontium, Phys. Rev. A **93**, 022709 (2016).
[37] The exact form of the Heisenberg-Langevin equation and the detailed derivation of it can be found in C. Gardiner and P. Zoller, *Quantum Noise*, 3rd ed. (Springer Berlin, Heidelberg, 2010); and C. Cohen-Tannoudji, J. Dupont-Roc, and G. Grynberg, *AtomPhoton Interactions* (John Wiley & Sons, Ltd, 1998).
[38] A. Peng, M. Johnsson, W. P. Bowen, P. K. Lam, H.-A. Bachor, and J. J. Hope, Squeezing and entanglement delay using slow light, Phys. Rev. A **71**, 033809 (2005).
[39] K. Qu and G. S. Agarwal, Fano resonances and their control in optomechanics, Phys. Rev. A **87**, 063813 (2013).
[40] P. Kolchin, Electromagnetically-induced-transparency-based paired photon generation, Phys. Rev. A **75**, 033814 (2007).
[41] K. E. Dorfman, F. Schlawin, and S. Mukamel, Nonlinear optical signals and spectroscopy with quantum light, Rev. Mod. Phys. **88**, 045008 (2016).
[42] C. Belthangady, S. Du, C.-S. Chuu, G. Y. Yin, and S. E. Harris, Modulation and measurement of time-energy entangled photons, Phys. Rev. A **80**, 031803(R) (2009).